ANL-7706

Argonne National Laboratory

VAPORIZATION DYNAMICS OF INITIALLY STATIC SUPERHEATED SODIUM

by

Ralph M. Singer and Robert E. Holtz

Printed in the United States of America
Available from
National Technical Information Service
U.S. Department of Commerce
Springfield, Virginia 22151
Price: Printed Copy $3.00; Microfiche $0.65

ANL-7706
Reactor Technology

ARGONNE NATIONAL LABORATORY
9700 South Cass Avenue
Argonne, Illinois 60439

VAPORIZATION DYNAMICS OF INITIALLY STATIC SUPERHEATED SODIUM

by

Ralph M. Singer and Robert E. Holtz

Reactor Analysis and Safety Division

September 1970

TABLE OF CONTENTS

LIST OF FIGURES

LIST OF FIGURES

NOMENCLATURE

A	Channel cross-sectional area
C	Channel circumference
c	Acoustic velocity
c_p	Specific heat
g	Gravitational acceleration
H	Displacement of liquid column
h_{fg}	Latent heat of vaporization
Ja	Jakob number, $\rho c_{p_\ell} \Delta T / \rho_v h_{fg}$
L_0	Initial height of liquid column above top of heater
L_1	Maximum displacement of liquid column
L_h	Length of zone of high heat flux
P	Pressure
q	Heat flux
r	Radius of active surface cavity
t	Time
T	Temperature
ΔT	Superheat, $T - T_S$
u,v	Velocity
x	Axial coordinate
α	Average void fraction
δ	Equivalent thickness of liquid film
θ	Contact angle
κ	Integration constant defined in Eq.
ρ	Liquid density
σ	Surface tension

Subscripts

F	Frozen
g	Gas blanket
gc	Gas in surface cavities
i	Impact conditions
ℓ	Bulk liquid
S,Sat	Saturation
v,V	Vapor
W	Wall
0	Initial conditions
*	Conditions defined by $H(t_*) = L_h$

Superscript

(*)	Collapse
(')	Conditions at maximum cavity deactivation

VAPORIZATION DYNAMICS OF INITIALLY STATIC SUPERHEATED SODIUM

by

Ralph M. Singer and Robert E. Holtz

ABSTRACT

Measurements of the patterns of vapor growth resulting during the transient boiling of initially static, nonuniformly superheated sodium in a vertical channel are presented and discussed. It is demonstrated that the single-slug vapor-growth model (in which the entire channel cross section is filled with vapor, except for a thin liquid film on the walls) may not be valid when the liquid temperature gradient normal to the channel axis is large and asymmetric, and/or the incipient boiling superheat is small. Under certain conditions, void fractions as low as 0.3 to 0.5 were observed. When the incipient superheat is large, the predictions of a simple vapor-slug-growth model compare favorably with the measured results. Experimental data on the vapor growth and collapse rates and the associated pressure transients are presented for boiling pressures up to about 1 atm and superheats up to about 180°C.

I. INTRODUCTION

An understanding of the vaporization dynamics of superheated sodium is of considerable importance in developing safety analyses of sodium-cooled, fast breeder reactors (LMFBR's). In this situation, where boiling is generally undesirable, the calculation of the safe operating limits of a reactor or the extent of damage resulting from postulated accidents is partially dependent upon knowledge of the mechanism and rate at which sodium may vaporize.

It is well-known that under normal circumstances liquids will boil when their temperatures slightly exceed the saturation level with the resultant generation of a large number of relatively small vapor bubbles. However, under certain circumstances (e.g., a heating surface highly wetted by the liquid, lack of nucleation sites, or rapid heating or depressurization transients), liquids can become superheated substantially above their normal boiling temperatures. When nucleation occurs under these conditions, the

first bubble that forms grows quite rapidly and increases the liquid pressure in its vicinity; this results in a suppression of nucleation at other possible sites. This phenomenon has been observed in liquid alkali metals[1-3] as well as in nonmetallic fluids.[4-6] Furthermore, if the liquid is in a channel (as opposed to a "pool"), the initially spherical vapor bubble will deform and grow primarily in the direction of the channel axis.

In these earlier experiments, either uniform heating[1-3] or depressurization[4-6] of a liquid in a circular tube was used to cause superheated boiling; these techniques resulted in either radially symmetric or radially uniform profiles of liquid temperature. As a result, the bubble that was formed was also radially symmetric and filled the entire tube cross section except for a thin liquid film remaining on the walls. Based on these results, several theoretical models of vapor-slug growth in sodium were developed, incorporating the observed symmetries.[7,8] However, the possibility of an asymmetric liquid temperature profile, causing the bubble to grow asymmetrically, was not examined. Both symmetric and asymmetric growth will be examined in this paper.

The patterns of vapor growth and growth rates in nonuniformly superheated sodium were measured at a variety of experimental conditions in the experimental apparatus described in Sect. II. Data are presented on the incipient boiling superheat of sodium in which an apparent heat-flux effect is discussed.

II. EXPERIMENTAL APPARATUS

The apparatus in which the vapor-growth and incipient-boiling measurements for sodium were made is shown in overall perspective in Fig. 1. Photographs of the vacuum vessel containing the test section and electron-beam gun are shown in Figs. 2 and 3; details of the measurement locations of the test section are sketched in Fig. 4. The sodium was contained in a vertical tube, made of Type 304 stainless steel, the lower section having a rectangular cross section, 9.5 x 25.4 mm, and a length of 500 mm; the upper section was a circular tube with an internal diameter of 17.5 mm. The cross-sectional area of the rectangular section was 241.3 mm^2, that of the tube being 240.5 mm^2. The total length of the tube was 4.3 m.

Low-power-density heaters along the length of the tube were used to establish and maintain a specified vertical temperature distribution, while an electron-bombardment heater was used to supply a large heat flux to a 50- to 90-mm section of one side of the lower rectangular portion of the tube (the back side of this portion of the rectangular tube was unheated). This type of heating arrangement was employed to assure that nucleation would occur in an essentially predetermined region and to simulate the axial temperature profiles expected away from the center of an LMFBR subassembly.

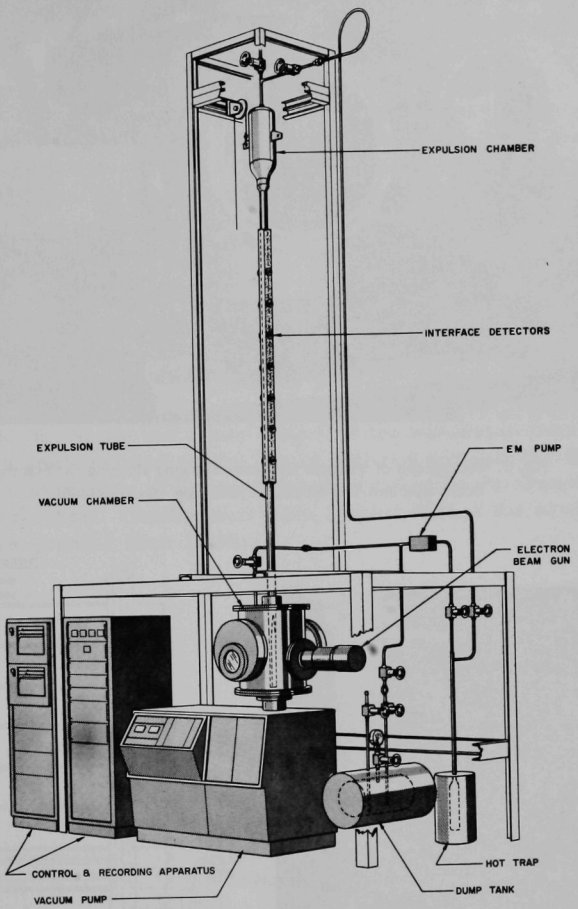

Fig. 1. Pictorial View of Apparatus for Studying Sodium Vapor Growth. ANL Neg. No. 112-7827A.

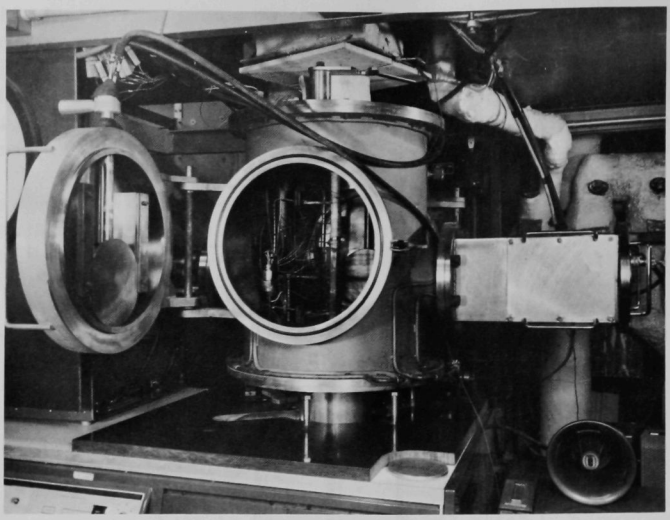

Fig. 2. Photograph of Vacuum Chamber Showing Housing for Electron-beam Gun and Test Section. ANL Neg No. 113-3000.

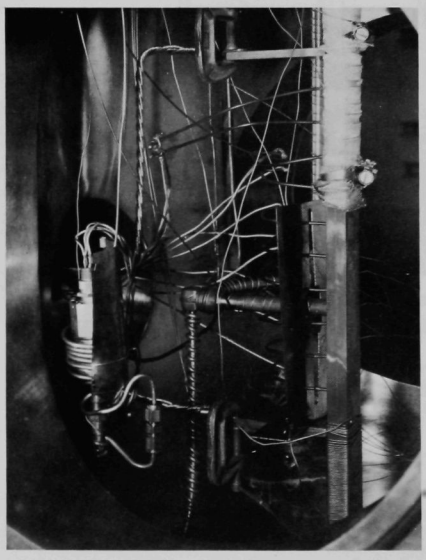

Fig. 3. Closeup Photograph of Test Section. ANL Neg No. 113-3003.

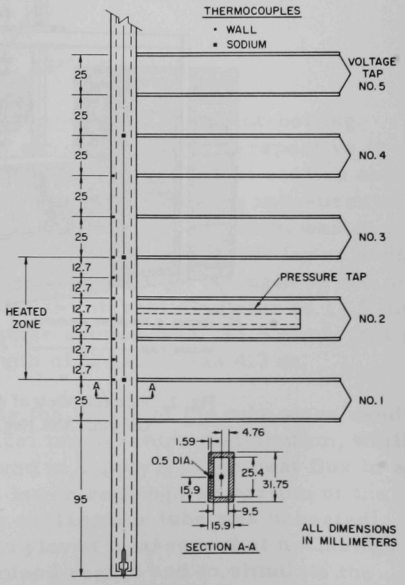

Fig. 4. Details of Measurement Locations on Test Section. ANL Neg. No. 113-3234.

Temperatures were measured using 1.6-mm-diameter, Inconel-sheathed, Chromel/Alumel thermocouples immersed in the sodium and imbedded in the tube wall. The pressure of the upper argon gas blanket was measured by a precision Bourdon-type pressure gauge, while the liquid pressure in the high heat-flux region was measured by a special, fast-response (~4 kHz) strain-gauge type of transducer mounted in a standoff for temperature protection. The position of the liquid-vapor (bubble) interface was detected by passing a lower-power, constant direct electrical current through the tube wall and sodium, and measuring the electrical potential at various locations along the length of tube. The displacement of the top of the liquid column (liquid-gas interface) above the growing vapor slug was measured by the use of specially designed, eddy-current type of coils (see Fig. 5). A high-frequency signal was sent to each of the driver coils, and an induced signal was then detected in each pickup coil; the magnitude of this induced signal is directly related to the electrical conductivity of the material between the driver and pickup coils. Thus, spacing the coils sufficiently far apart to avoid any extraneous intercoil pickup allowed a direct indication of the position of the upper liquid-gas interface as it passed through each coil field. The coils were located at intervals of 76 mm along the upper length of the expulsion tube. Analysis of the type of signal induced as the liquid entered and left the field of a coil indicated a precision of approximately ±5 mm in the transient location of the liquid interface. Calibration tests indicated that the response of these coils was greater than 1 kHz.

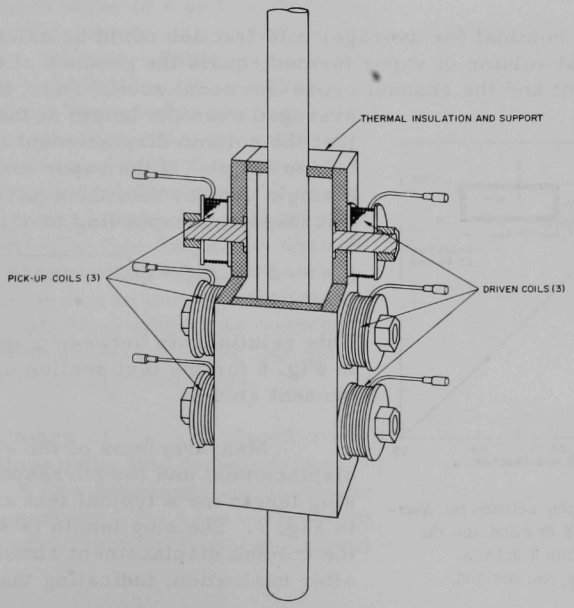

Fig. 5. Schematic of Liquid-level Detector. ANL Neg. No. 112-9472.

A typical experiment was conducted in the following manner: (1) the gas-blanket pressure was set at some level, (2) the low-power-density heaters were then used to establish a prescribed vertical temperature distribution, and (3) the electron-bombardment heater was then turned on and maintained at a constant power until either steady or quasi-steady boiling was observed. The system would then be allowed to cool down and a new test initiated. All data were continuously recorded on either oscillographs or strip-chart instruments.

III. EXPERIMENTAL RESULTS

A. Patterns of Vapor Growth

Since direct visual observations of the boiling liquid could not be made, the patterns of vapor growth were inferred from indirect measurements. The two measurements that were primarily used for this purpose were (i) the total displacement of the liquid column and (ii) the axial motion of the liquid-vapor (bubble) interface. The measurements of the electrical potential along length of the tube prior to and during vapor growth indicated that the flow regime was most likely that of a single vapor bubble expanding against the liquid column for incipient-boiling bulk-liquid superheats greater than about 10°C. However, these measurements could not distinguish between a single bubble and region of a high void fraction (i.e., bubbly flow) if, in both cases, the walls remained wet.

The nominal (or average) void fraction could be calculated by noting that the total volume of vapor formed equals the product of the column displacement and the channel cross-sectional area. Thus, the void fraction averaged over the length of the bubble, α, is just the column displacement divided by the bubble length. If the vapor formed is that of a single bubble, then the equivalent liquid-film thickness corresponding to α is just

$$\delta = \frac{1}{8}\left[C - \sqrt{C^2 - 16A(1-\alpha)}\right]. \qquad (1)$$

This relationship between α and δ is illustrated in Fig. 6 for the test section used in the present studies.

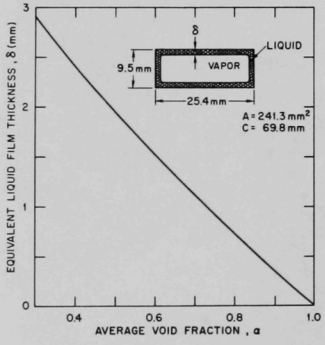

Fig. 6. Relationship between the Average Void Fraction and the Liquid-film Thickness. ANL Neg. No. 900-136.

Measurements of the sodium-column displacement and the corresponding vapor-slug length for a typical test are presented in Fig. 7. The slug length is seen to exceed the column displacement almost immediately after nucleation, indicating that the vapor slug

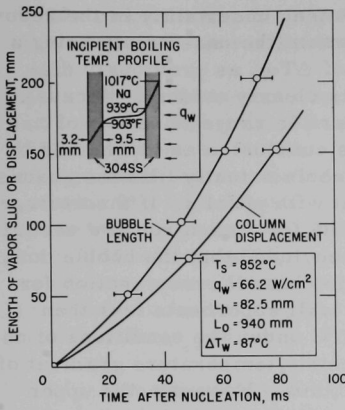

Fig. 7. Variation of Vapor Slug and Displacement Length with Time. ANL Neg. No. 113-3200 Rev. 2.

does not fill the channel cross section. The uncertainties in the time coordinate indicated in Fig. 7 arise from the difficulty in determining the precise instant of nucleation, which results in some error in relating the transient bubble length and column displacement to the same time scale. The criterion chosen in this work for the inception of vapor growth (i.e., nucleation) was the instant at which the liquid pressure started to increase. At large incipient superheats (i.e., $\Delta T_W \gtrsim 100°C$), the pressure rise was relatively abrupt at nucleation, resulting in an error in the determination of zero time of about ±1 to ±2 msec. However, at smaller superheats (i.e., $\Delta T_W \lesssim 50°C$), the initial pressure rise was more gradual, resulting in an error in the zero-time location of ±5 to ±8 msec.

Unfortunately, the calculation of the average void fraction from the bubble-length and column-displacement data is extremely sensitive to these errors in time. As an illustration of this sensitivity, the average void fraction as calculated from the data of Fig. 7 with the indicated error in the relative zero time of ±5 msec is shown in Fig. 8. The circles indicate the mean value of α and the bars indicate the possible range of α based on the ±5-msec error. Because of this large uncertainty in these calculations, it is difficult to draw any hard and fast conclusions, i.e., it is not really clear whether or not the bubble initially filled the channel under these particular conditions. However, it does seem clear that as the bubble grows larger, the void fraction decreases, indicating that the bubble does not continually fill the channel as it grows axially. This, of course, is due in part to a diminished vapor-growth rate (and ultimately condensation) as the bubble grows out of the high-heat-flux zone into cooler surroundings.

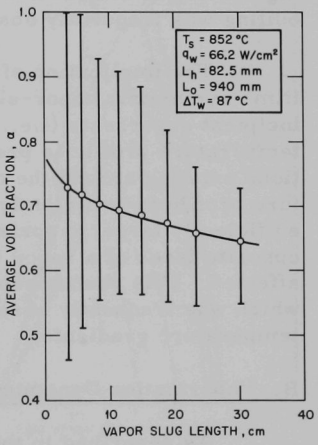

Fig. 8. Variation of Average Void Fraction with Slug Length. ANL Neg. No. 900-137.

A summary of the calculated average void fractions using this technique is presented in Fig. 9 as a function of the incipient-boiling wall superheat ΔT_W. Again, the large error in the void fraction resulting from a

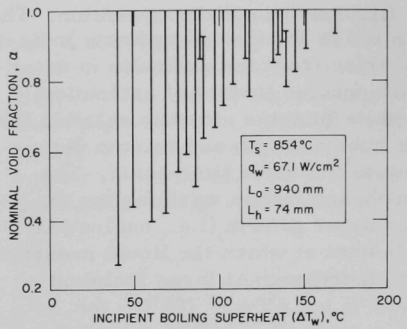

Fig. 9. Variation of Average Void Fraction with Superheat. ANL Neg. No. 900-363.

±1 to ±8-msec uncertainty in the zero-time location (the uncertainty being a function of ΔT_W, as previously discussed) is clearly evident. Because of the possible range of values of α, a definitive conclusion as to whether or not the bubble actually fills the channel is fraught with pitfalls. If the average values of α from each run are used, it may be concluded that the bubble does not fill the channel cross section for incipient wall superheats less than about 100°C under the conditions of an axisymmetric temperature gradient of about 4°C/mm. However, the upper limits of α indicate that the cross section may possibly be filled with vapor for superheats as low as 40°C. But, in general, it does appear that as the incipient superheat is reduced, the average void fraction tends to become smaller, indicating that the vapor bubble does not fill the channel cross section.

This conclusion is reinforced by the further observation that for incipient wall superheats less than about 10°C with wall heat fluxes from 55 to 290 W/cm^2, no vapor slug was formed (as indicated by the voltage taps), and the sodium went directly into stable nucleate boiling. In the higher ranges of heat flux (greater than about 200 W/cm^2), subcooled boiling was frequently observed.

The implication of this interpretation of the data is that the "thin-film" symmetric vapor-slug models of Refs. 7 and 8 may not apply at low incipient superheats (i.e., less than about 20-50°C) when an asymmetric temperature profile is present, because of the asymmetric thermal conditions existing around the circumference of the vapor slug. If the temperature profile is sufficiently asymmetric, i.e., the temperature gradient sufficiently large, vaporization and condensation can possibly occur at opposite faces of a vapor bubble and its net growth rate will be obviously affected. This phenomenon is most vividly apparent in subcooled boiling, which was frequently observed at the larger heat fluxes (i.e., at larger temperature gradients).

B. Vaporization Dynamics

As described in the previous section, the vapor-growth pattern was most likely that of a single bubble that filled 40% to essentially 100% of the channel cross section, depending upon the incipient-boiling superheat and the temperature gradient in the liquid. In this section, the vaporization

dynamics of the vapor slug will be discussed, and its dependence upon the superheat and saturation conditions delineated.

In the tests reported herein, the temperature of the liquid sodium far from the high-heat-flux zone was always maintained at approximately 550°C (in order to simulate fast breeder reactor conditions), resulting in a large axial temperature gradient at incipient boiling. Only the liquid in and near the high-heat-flux region was superheated; the liquid above and below was subcooled, as illustrated by typical temperature profiles at the instant of boiling in Figs. 16-22. The result of this temperature gradient was to cause an ultimate collapse (condensation) of the vapor slug as it grew into the cooler regions of the channel. This vapor collapse resulted in rather large pressure shocks that are discussed in a later section.

Measurements of the liquid-column displacement caused by the vapor-slug growth and collapse for several saturation temperatures and a variety of incipient bulk superheats are shown in Figs. 10 through 15. The maximum displacement and growth rate of the vapor slug clearly increase as the incipient bulk-liquid superheat increases. Also shown in Figs. 12, 13, and 15 are secondary vaporizations following the collapse of the initial vapor slug; this second-growth phenomenon occurred somewhat sporadically and was not nearly as reproducible as the initial growth behavior.

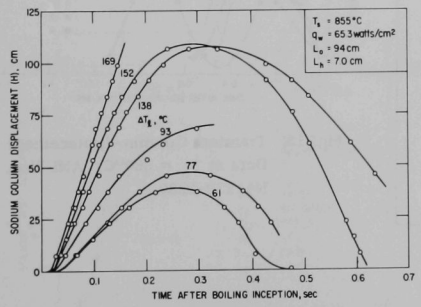

Fig. 10. Transient Column-displacement Data at T_S = 855°C. ANL Neg. No. 113-2282 Rev. 2.

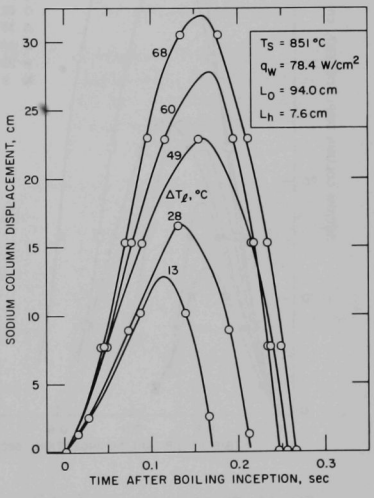

Fig. 11. Transient Column-displacement Data at T_S = 851°C. ANL Neg. No. 113-3228.

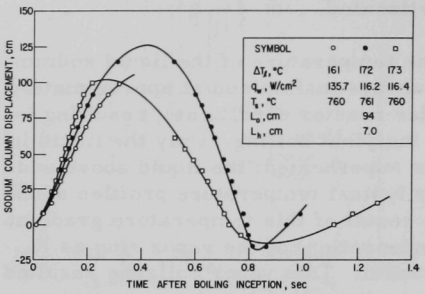

Fig. 12. Transient Column-displacement Data at $T_S \tilde{=} 760^{o}C$ and $q_w > 155$ W/cm^2. ANL Neg. No. 113-2284 Rev. 1.

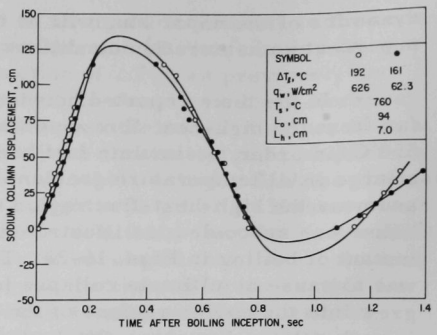

Fig. 13. Transient Column-displacement Data at $T_S = 760^{o}C$ and $q_w < 65$ W/cm^2. ANL Neg. No. 113-2280 Rev. 1.

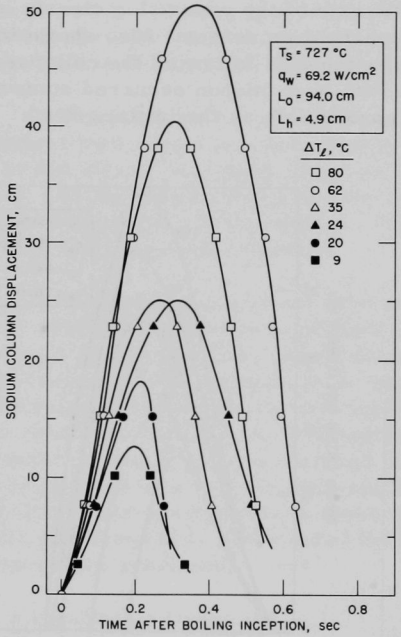

Fig. 14. Transient Column-displacement Data at $T_S = 727^{o}C$. ANL Neg. No. 113-3236.

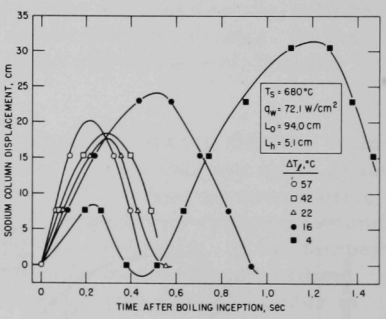

Fig. 15. Transient Column-displacement Data at $T_S = 680^{o}C$. ANL Neg. No. 113-3230.

At large incipient-boiling superheats, the vapor slug has been shown to essentially fill the channel cross section; thus, a simple model of vapor growth (as described in Appendix A) based upon the inertia of the liquid column and assuming that vaporization occurs only in the high-heat flux region may be expected to agree reasonably well with the measurements. The comparison of the predicted and measured column displacements are shown in Figs. 16 through 22 for several saturation temperatures and wall heat fluxes. As would be expected, the model fails to predict the behavior at small incipient bulk-liquid superheats because of the apparent nonfilling of the channel with vapor. The inertia-limited model with a constant driving pressure based upon the bulk-liquid superheat (see Eq. 8 in Appendix A) is

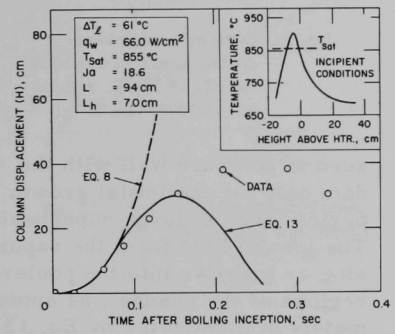

Fig. 16. Comparison of Column-displacement Data with Model for $\Delta T_L = 61^oC$. ANL Neg. No. 113-2794 Rev. 3.

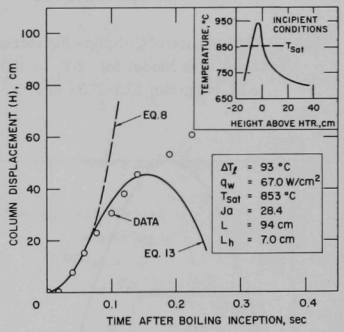

Fig. 17. Comparison of Column-displacement Data with Model for $\Delta T_L = 93^oC$. ANL Neg. No. 113-2795 Rev. 2.

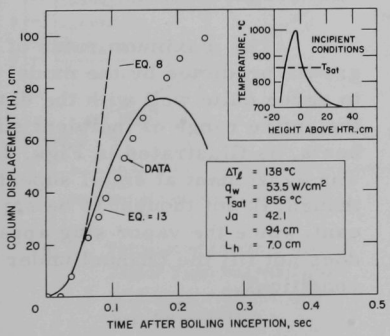

Fig. 18. Comparison of Column-displacement Data with Model for $\Delta T_L = 138^oC$. ANL Neg. No. 113-2802 Rev. 2.

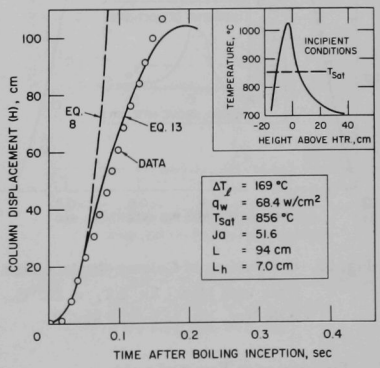

Fig. 19. Comparison of Column-displacement Data with Model for $\Delta T_L = 169^oC$. ANL Neg. No. 113-2798 Rev. 3.

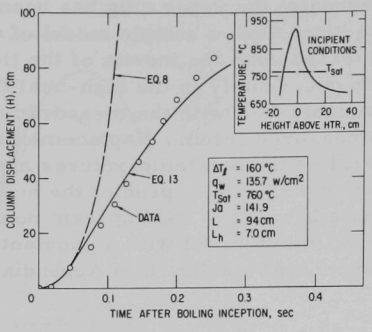

Fig. 20. Comparison of Column-displacement Data with Model for $\Delta T_L = 160^{\circ}C$. ANL Neg. No. 113-2793 Rev. 2.

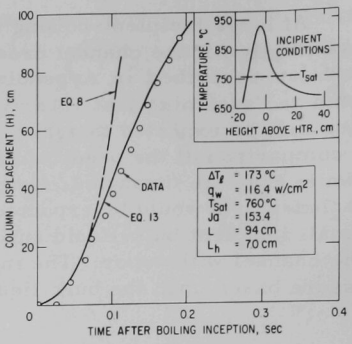

Fig. 21. Comparison of Column-displacement Data with Model for $\Delta T_L = 173^{\circ}C$. ANL Neg. No. 113-2799 Rev. 2.

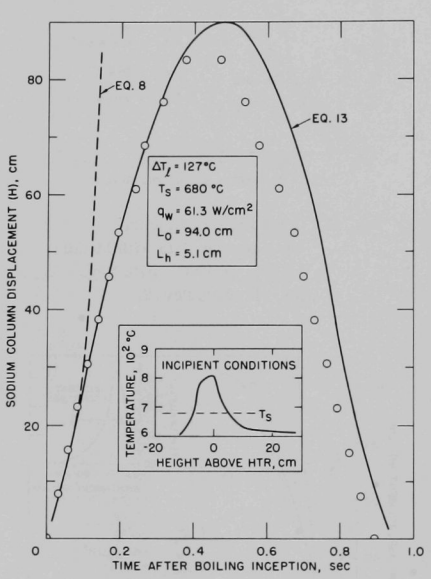

Fig. 22. Comparison of Column-displacement Data with Model for $\Delta T_L = 127^{\circ}C$. ANL Neg. No. 113-3225 Rev. 2.

seen to compare well with the data only for the initial growth period, even at large superheats. The loss of heat from the vapor slug as it grows into the cooler regions of the channel, as approximately accounted for by Eq. 13 in Appendix A, is seen to reduce markedly the rate of slug growth. As would be expected, the collapse of the slug is not well represented; some qualitative agreement between the data and the model was noted (see Fig. 22), but this was thought to be fortuitous.

The maximum rates of vapor growth predicted by the model seem to agree quite well with the data over the entire range of incipient superheats, as illustrated in Figs. 23-25. The agreement at small superheats, though, is not thought to be significant, since the vapor slug apparently does not fill the channel under these conditions.

C. Pressure Transients

The transient liquid pressure measured during the growth and collapse of the vapor slug was qualitatively quite similar to that observed during the rapid transient boiling of water and other fluids in a vertical

channel.[9] As illustrated in Fig. 26, the pressure would initially rise to a maximum during the vapor growth and then gradually drop to a level considerably below that of the upper gas-blanket pressure during vapor condensation. When the upper liquid column ultimately impacted with the lower column following collapse of the slug, a very sharp rise in pressure resulted. The rise time of the initial pressure increase was typically 10-40 msec, while that of the impact pressure was about 0.1 to 0.3 msec.

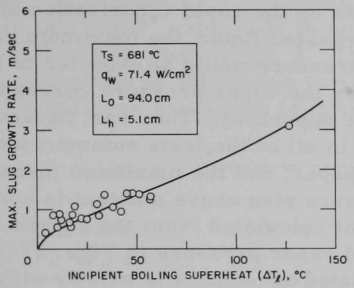

Fig. 23. Variation of Maximum Growth Rate of Vapor Slug with Superheat at T_S = 681°C. ANL Neg. No. 113-3238.

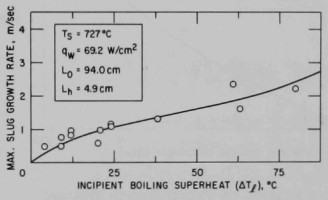

Fig. 24. Variation of Maximum Growth Rate of Vapor Slug with Superheat at T_S = 727°C. ANL Neg. No. 113-3227.

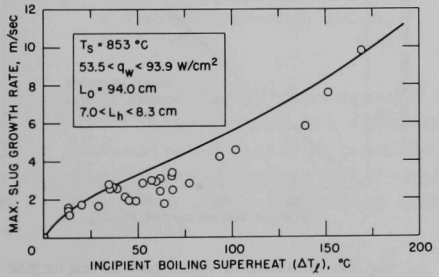

Fig. 25. Variation of Maximum Growth Rate of Vapor Slug with Superheat at T_S = 853°C. ANL Neg. No. 113-3229.

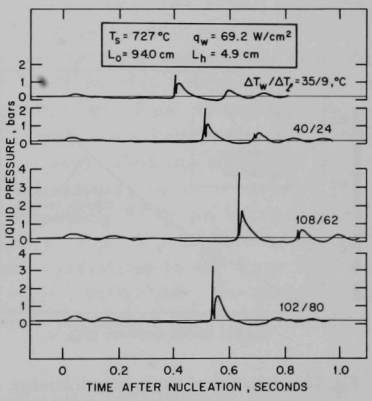

Fig. 26. Typical Pressure Transients during Vapor Growth and Collapse. ANL Neg. No. 900-139.

An examination of the initial pressure rises in Fig. 26 indicates a possible self-pressurization effect shortly after the first pressure peak.

This phenomenon was predicted in the analyses in Refs. 7 and 8, and is caused by a buildup of the vapor pressure by continued vaporization at higher and higher temperatures at a faster rate than the vapor slug can expand. The measurements indicate that the extent of the self-pressurization of the vapor slug increases at larger superheats and, in fact, does not occur at low superheats.

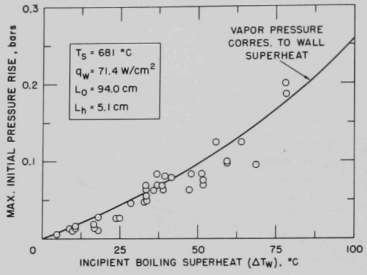

Fig. 27. Variation of Vapor-growth Pressure Rise with Superheat for T_S = 681°C. ANL Neg. No. 113-3231 Rev. 1.

Since the initial pressure rise is caused by the rapid vaporization of the superheated liquid, the maximum value of this pressure would be expected to be limited by the vapor pressure corresponding to the superheat. This was, in fact, the case in all of the tests summarized in this paper, and the maximum measured pressure rise above ambient is compared to that calculated from the superheated-liquid vapor pressure in Figs. 27-29. The indicated agreement is mostly within the estimated experimental accuracy of the pressure measurements (±0.1 bar).

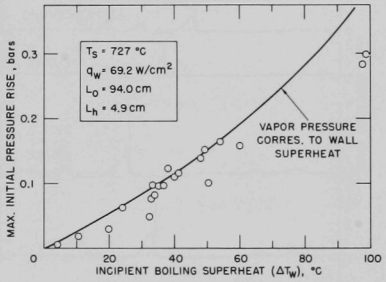

Fig. 28. Variation of Vapor-growth Pressure Rise with Superheat for T_S = 727°C. ANL Neg. No. 113-3233 Rev. 1.

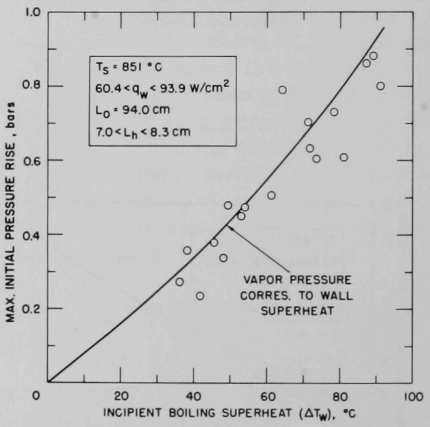

Fig. 29. Variation of Vapor-growth Pressure Rise with Superheat for T_S = 851°C. ANL Neg. No. 113-3232 Rev. 1.

As indicated in Appendix B, the magnitude of the pressure rise due to vapor collapse is expected to be a function of the gas-blanket pressure (or liquid subcooling) and the maximum displacement of the liquid column, L_1, according to the relationship

$$P^* = \rho c \left[\frac{L_1}{2} \left(\frac{P_g}{\rho L_0} + g \right) \right]^{1/2} . \qquad (2)$$

From this equation it would be expected that a plot of $P^*/\sqrt{L_1}$ versus P_g for a fixed value of L_0 and a specific fluid should provide a reasonable correlation of the experimental data. However, plots of P^* versus P_g or P^* versus liquid subcooling appeared to correlate the data just as adequately. Therefore, it was decided that the latter correlation would be used in this paper, especially in order to facilitate comparison of the present data with that of Ref. 2. These results are shown in Fig. 30, where the strong effect of subcooling (or, equivalently, the gas-blanket pressure) upon the collapse pressures is illustrated.

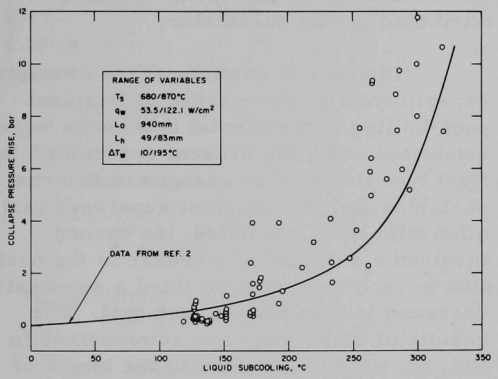

Fig. 30. Variation of Pressure Rise due to Vapor Collapse with Subcooling. ANL Neg. No. 113-3271.

D. Incipient-boiling Superheats

Many parameters appear to have significant effect upon the incipient-boiling superheat of sodium,[10] for example, the pressure-temperature history of an experimental apparatus, the boiling pressure, heat flux, liquid purity, dissolved and entrained gas content, and liquid velocity. The effect that has received perhaps the most inconsistent and conflicting experimental evidence is that of the heat flux. For example, data have been presented indicating that the incipient superheat may be decreased,[2] increased or decreased,[11] increased,[12] or unaffected[13] by an increase in the heat flux; these results are summarized in Fig. 31. In this section, it will be demonstrated that it is possible that variations in the heat flux were not responsible for the observed changes in the superheat; the mobility of inert gas between active nucleation sites and the liquid can result in the observed behavior.

Since the solubility of inert gas in liquid alkali metals increases with increasing temperature, gas will be lost from gas- and vapor-filled nucleation sites on the heated wall during the heating prior to and during boiling, and will be gained by the sites during the cooling between tests. Since the incipient-boiling superheat will increase if the amount of inert gas in a nucleation site is decreased as indicated by the relation between the pressure and surface tension forces,

$$P_v(T_w) - P_\ell = \frac{2\sigma(T_w)\cos[\theta(T_w)]}{r} - P_{gc}, \qquad (3)$$

it is clear that the gas partial pressure in the sites, P_{gc}, must be maintained constant during a sequence of tests or this gas effect may mask other phenomena affecting the superheat. This is a difficult experimental requirement since there is no way to measure the inert gas partial pressure in the microscopic nucleation sites directly; thus, the usual procedure is to allow a certain length of time between tests to permit the system to return to its initial conditions. However, if this time is insufficient to allow the cavity-inert gas partial pressure, P_{gc}, to reattain its initial value, each successive test will be run with a reduced cavity gas pressure. This causes the incipient-boiling superheat to increase with each test; if some other external parameter was varied during these tests, the changing superheat could be erroneously attributed to that parameter.

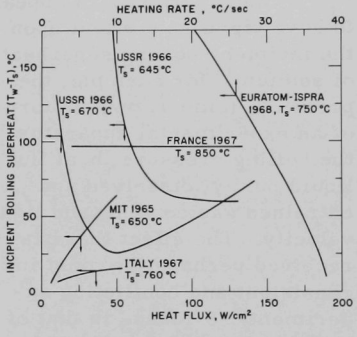

Fig. 31. Reported Effects of Heat Flux upon the Incipient-boiling Superheat. ANL Neg. No. 900-105.

In order to examine these concepts experimentally, three types of incipient pool-boiling experimental sequences were conducted using the present apparatus: the first type involved no changes of external variables and the incipient superheat variation with time was noted, the second involved a successive increase in the heat flux in each test, and the third a successive decrease in heat flux in each test. The results of these tests are summarized in Fig. 32, where t_F refers to the length of time that the sodium was frozen prior to the start of testing.

During tests in which no external variables were changed (the upper curves in Fig. 32), the incipient superheat increased with time. The second and third tests also indicated the same increase of superheat with time; however, because of the direction of sequential changes of heat flux, apparently opposite effects of the heat flux upon the incipient superheat resulted. It is clear from these tests that the observed changes in the superheat were not directly caused by changes in the heat flux; variations in the cavity inert gas pressure seem to provide a very plausible explanation. The predicted value of the superheat with $P_{gc} = 0$ for the second and third tests using the model of Holtz[14] was 97°C, which agrees reasonably well with the asymptotic measured values. Therefore, based on these conclusions, previously reported heat-flux effects upon the incipient superheat must be treated with considerable caution.

An additional observation from these data is that the measured incipient boiling wall superheat for the first test (i.e., the first heating transient following a period of steady, nonboiling heating) is usually quite

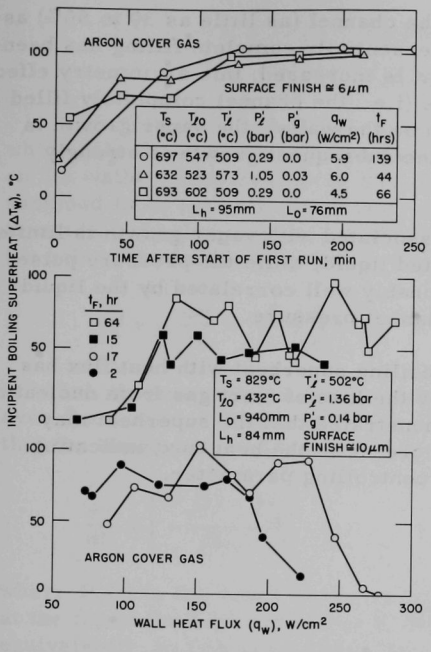

Fig. 32. Variation of Superheat with Time and Heat Flux. ANL Neg. No. 113-3201.

small, in many cases, zero. This finding may have considerable importance to reactor applications, since the reactor would be expected to operate for a considerable length of time at steady state prior to an approach to boiling caused by some accident. Thus, for reactor safety applications, the value of the incipient superheat that is of paramount importance is that which occurs following just such a lengthy period of nonboiling. Under the conditions of these tests (e.g., no flow), this superheat was quite small. Although it would be quite attractive to extrapolate this finding immediately to actual LMFBR conditions, one must be aware of the differences between these tests and those occurring in a reactor, particularly the lack of flow and the frozen condition of the sodium prior to heating. The influence of flow will be examined in future tests.

A summary of the asymptotic incipient-boiling wall-superheat data (i.e., the values of ΔT_W obtained after a number of preliminary boiling runs) is presented in Fig. 33 and compared to the theoretical predictions of the pressure-temperature history model.[14] Although a considerable scatter is noted, the general trend of the data follows the predicted behavior.

IV. CONCLUSIONS

In summary, the flow pattern resulting from the vaporization of nonuniformly superheated sodium in a vertical channel has been shown to most likely be that of a single bubble if the incipient-boiling bulk-liquid superheat is greater than about 10°C. However, it appears that an asymmetric radial temperature profile may result in the vapor bubble filling

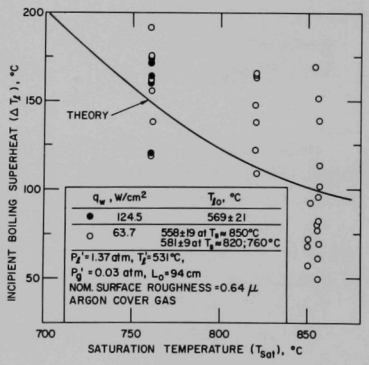

Fig. 33. Variation of Superheat with Saturation Temperature. ANL Neg. No. 113-2792 Rev. 1.

only a portion of the cross section of the channel (as little as 30 to 50%) as opposed to the symmetric case where essentially complete filling has been observed.[1-3] As the incipient superheat is increased, this asymmetry effect diminishes. For the symmetric bubble (i.e., the channel completely filled with vapor except for a thin liquid film on the walls), the vapor growth is initially limited by liquid inertia, but the subsequent growth is strongly affected by heat transfer.

The maximum pressure rise associated with vapor growth is limited by the vapor pressure of the superheated liquid, while the pressure pulse resulting from vapor collapse is reasonably well correlated by the liquid subcooling or, equivalently, the gas-blanket pressure.

The variation of the incipient-boiling superheat with heat flux has been shown to be most likely caused by the loss of inert gas from nucleation sites. It has been experimentally demonstrated that the superheat may either increase or decrease with an increase in the heat flux, indicating that the heat flux is not necessarily a controlling parameter.

APPENDIX A

Model of Vapor-slug Growth

In this model, it is assumed that the vapor grows as a single bubble which fills the entire channel cross section except for a thin liquid film on the walls. Vaporization of this liquid film in the high-heat-flux zone is assumed to be the primary driving factor in the growth of the bubble. The transient, one-dimensional momentum equation for the liquid column above (or below) the bubble may be written as

$$\frac{\partial u}{\partial t} + u \frac{\partial u}{\partial x} = -\frac{1}{\rho} \frac{\partial P}{\partial x} + g, \tag{4}$$

in which viscous terms have been neglected. If this equation is integrated over the length of the liquid column (i.e., from $x = 0$ to $x = L_0$), assuming that the liquid is incompressible, there results

$$\frac{du}{dt} = \left[\frac{P_v(t) - P_g}{\rho L_0} \right] - g, \tag{5}$$

where $P_v(t)$ is the vapor pressure in the bubble and P_g is the gas pressure at the top of the liquid column. If $H(t)$ is the length of the vapor bubble (or, equivalently, in this case, the column displacement), the initial conditions on $H(t)$ for the period of slug growth are

$$u = \frac{dH}{dt} = 0; \quad H = 0 \text{ at } t = 0. \tag{6}$$

However, in order to integrate Eq. 5, the variation of the bubble pressure P_v with time must be specified. This is accomplished by relating P_v to the temperature and volume of the vapor phase through an equation of state, and determining the vapor temperature through the equations of energy conservation.

As a first approximation, it will be assumed that while the vapor bubble remains within the high-heat-flux zone, the vaporization of the liquid film is sufficiently rapid so as to maintain the bubble pressure at the value corresponding to the initial superheated bulk liquid temperature, i.e., at $P_v(T_\ell)$. As the bubble expands out of this zone into cooler regions, where the evaporation rate is much smaller (in fact it can be zero or negative), its pressure will be allowed to vary according to the ideal gas law. For the one-dimensional case studied here, this results in the pressure function

$$P_v = P_v(T_\ell), \quad 0 < H(t) < L_h; \tag{7a}$$

$$= P_v(T_\ell) L_h / H(t), \quad H(t) > L_h, \tag{7b}$$

where L_h is the length of the high-heat-flux zone.

Therefore, for values of t such that $H(t) < L_h$, Eqs. 5, 6, and 7a can be directly solved to yield

$$H(t) = \left(\frac{t^2}{2}\right)\left[\frac{P_v(T_\ell) - P_g}{\rho L_0}\right] - g \; ; \qquad t < t_*, \tag{8}$$

where

$$H(t_*) = L_h \tag{9}$$

determines the value of t_*. From Eq. 8, t_* is evaluated as

$$t_* = \left[\frac{2\rho L_0 L_h}{P_v(T_\ell) - P_g - \rho L_0}\right]^{1/2} \tag{10}$$

For $t > t_*$, Eqs. 5 and 7b become

$$\rho L_0 \frac{d^2H}{dt^2} = \frac{P_v(T_\ell)L_h}{H} - (P_g + \rho g L_0); \qquad t > t_*. \tag{11}$$

By suitable manipulations, the first and second integrals of this equation can be obtained as

$$\frac{dH}{dt} = \left\{\left[\frac{2L_h P_v(T_\ell)}{\rho L_0}\right] \ell n \; H(t) - 2\left(\frac{P_g}{\rho L_0} + g\right) H(t) + \kappa\right\}^{1/2} \tag{12}$$

and

$$H(t) = L_h + \int_{t_*}^{t} \left\{\left[\frac{2L_h P_v(T_\ell)}{\rho L_0}\right] \ell n \; H(t') - 2\left(\frac{P_g}{\rho L_0} + g\right) H(t') + \kappa\right\}^{1/2} dt'. \tag{13}$$

This Voltera-type integral equation can then be solved for H(t) by either iteration or numerical approximation. The latter technique was used in this paper. The value of κ as determined from the initial conditions is

$$\kappa = t_*^2\left[\frac{P_v(T_\ell) - P_g}{\rho L_0} - g\right]^2 - \left[\frac{2L_h P_v(T_\ell)}{\rho L_0}\right] \ell n \; L_h + 2\left(\frac{P_g}{\rho L_0} + g\right) L_h, \tag{14}$$

and the maximum value of dH/dt (occurring at $d^2H/dt^2 = 0$) is

$$\left[\frac{dH}{dt}\right]_{max} = \left\{\left[\frac{2L_h P_v(T_\ell)}{\rho L_0}\right] \ell n\left[\frac{L P_v(T_\ell)}{\rho g L_0 + P_g}\right] - \frac{2P_v(T_\ell)}{\rho} + \kappa\right\}^{1/2}. \quad (15)$$

APPENDIX B

Vapor-collapse Pressures

As the vapor slug grows into the cooler upper regions of the channel, condensation will occur, ultimately causing the expelled liquid column to fall back and impact upon the stationary lower liquid column. The pressure rise resulting from this impact is usually much larger than that occurring during vapor growth, although of a much shorter duration. In order to estimate the magnitude of these collapse or impact pressures, as well as to determine the parameters affecting their value, a simplified analysis is presented here.

Consider a liquid column of length L_0 initially separated from a lower, stationary column by the distance L_1. A pressure P_g is applied to the top of the upper column and the pressure between the two columns is zero (corresponding to a completely condensed vapor bubble); thus, the upper column will be accelerated toward the lower column according to the relation

$$\rho L_0 \frac{du}{dt} = P_g + \rho g L_0, \tag{16}$$

with the boundary condition

$$u = 0 \text{ at } t = 0. \tag{17}$$

Equation 16 has the solution

$$u = \left(\frac{P_g}{\rho L_0} + g \right) t. \tag{18}$$

The velocity of the column immediately prior to impact (i.e., after it has fallen a distance L_1) is

$$u_i = \left[2L_1 \left(\frac{P_g}{\rho L_0} + g \right) \right]^{1/2}. \tag{19}$$

After the impact, the upper part of the liquid column continues to fall, compressing the liquid in the region of the impact position and increasing the pressure in this region. The resulting pressure wave then propagates upward and downward in the channel with the sonic velocity c. Thus, after a time t following impact, a length 2ct of the liquid has been pressurized to some value, P*, and the velocity of the liquid inside this pressurized length is some value v. An equating of the momentum of the mass of liquid, $2\rho Act$, that is pressurized to P* at time t after the impact to the momentum of the same mass immediately prior to impact results in

$$(2\rho Act)v = (\rho Act)u_i + 0 \tag{20}$$

or

$$v = u_i/2. \tag{21}$$

Thus,

$$v = \left[\frac{L_i}{2}\left(\frac{P_g}{\rho L_0} + g\right)\right]^{1/2}, \tag{22}$$

and the impulse given to the initially stationary lower liquid column is

$$P^*At = (\rho Act)v - 0 \tag{23}$$

or

$$P^* = \rho cv. \tag{24}$$

Therefore, the impact pressure is just

$$P^* = \rho c\left[\frac{L_i}{2}\left(\frac{P_g}{\rho L_0} + g\right)\right]^{1/2}. \tag{25}$$

Referring this analysis to the experiment described in this paper, L_1 is the maximum column displacement during vapor growth, and P_g is the gas-blanket pressure. The value of L_1 will depend upon the initial superheat, the gas-blanket pressure, the length of the upper liquid column, and the type of liquid, so that the impact pressure rise will be a function of all of these variables, i.e.,

$$P^* = f(\Delta T, P_g, L_0, \text{liquid properties}). \tag{26}$$

During the experiments reported on in this paper, the temperature of the upper liquid column was maintained at a fixed, subcooled value; thus, as the gas-blanket pressure was increased, the saturation temperature would increase, resulting in an increase in the subcooling. Therefore, an empirical correlation would be justified using either the gas pressure or the subcooling as interchangeable parameters.

An application of the equation derived for P^* to a number of experimental tests revealed that the measured pressures were smaller than the predicted pressures by a factor of 3 to 5. This discrepancy is apparently

due to several factors, one of which is the assumption of complete vapor collapse. Since heating was continued during the collapse, it is likely that some vapor was present in the heated zone as the liquid column reentered. This vapor presence was verified by pressure measurements of about 0.02 to 0.08 bar (absolute) during collapse; the pressure never dropped to zero. The effect of the presence of this vapor would be to cushion the impact, i.e., reduce its intensity. Additionally, the frequency of the pressure pulses (about 1 to 3 kHz) approached the resonant frequency of the pressure standoff tube (about 4 kHz), resulting in possibly severe errors in the measured pressure peaks. The measurements are thought to be reasonably correct, however, since they agree fairly well with those measured independently and reported in Ref. 2.

APPENDIX C

Characteristics of Boiling Surface

After the completion of the boiling experiments, the test section was cut out of the system and its surface characteristics examined. Photomicrographs of the channel cross section at several locations are shown in Fig. 34. The effects caused by boiling sodium are readily apparent by comparing the views of location 1 (untouched by sodium) and location 2 (in contact with sodium). No conclusions as to this observation are given here, as these photomicrographs are intended only for general information.

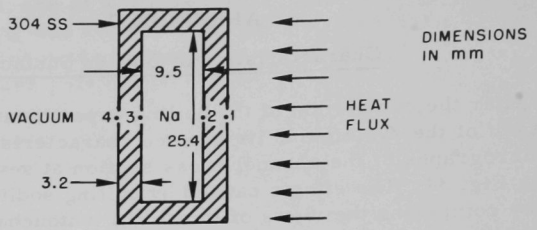

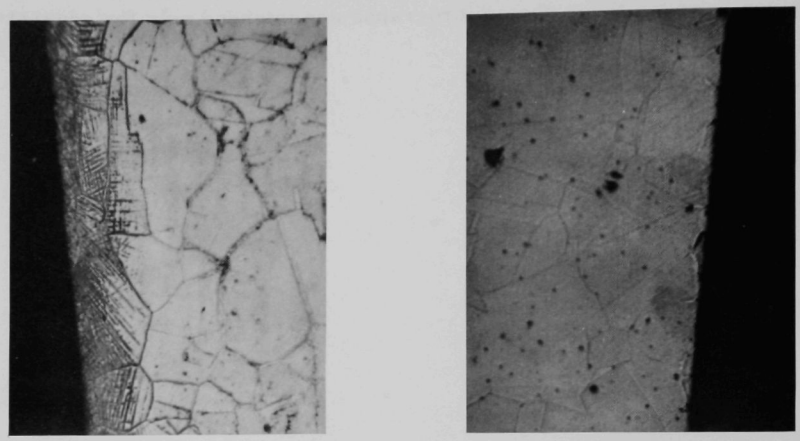

Fig. 34. Photomicrographs of Cross Sections of Boiling Channel. ANL Neg. No. 113-2222 Rev.2.

ACKNOWLEDGMENTS

We would like to take this opportunity to express our appreciation to Mr. Hubert R. Niemoth for his work in the design of much of the experimental apparatus, and to him and Mr. Ralph Moses for their efforts in the collection of data. We also appreciate the discussions held with Hans K. Fauske concerning the interpretation of the results.

REFERENCES

1. Spiller, K. H., *et al.*, *Überhitzung und Einzelblasenejektion bei der Verdampfung von stagnierendem Flussigmetallen*, Atomkernergie *12*, 111 (1967).

2. Spiller, K. H., Perschke, D., and Grass, G., *Überhitzen und Einzelblasenejektion von stagnierendem Natrium*, Atomkernergie *13*, 245-51 (1968).

3. Schlechtendahl, E. G., *Sieden des Kuhlmittels in natriumgekuhlten schnellen Reaktoren*, Gesellschaft fur Kernforschung (Karlsruhe) Report KFK 1020 (1969); also as EUR-4302d.

4. Kosky, P. G., *Bubble Growth Measurements in Uniformly Superheated Liquids*, Chem. Eng. Sci. *23*, 695 (1968).

5. Fette, P., *Simulation der Kuhlmittelejektion in natriumgekuhlter Brutreaktoren durch Experimente mit Wasser*, Gesellschaft fur Kernforschung (Karlsruhe) Report KFK-940 (1969); also as EUR-397d.

6. Grolmes, M. A., Fauske, H. K., and Lambert, G. A., *Superheat Expulsion in Single and Multipin Channels--Simulation of Blocked Subassembly Voiding*, Trans. ANS *12*(2), 907 (1969).

7. Schlechtendahl, E. G., *Die Ejektion von Natrium aus Reaktorkuhlkanalen*, Nukleonik *10*, 270-274 (1967).

8. Cronenberg, A. W., Fauske, H. K., and Bankoff, S. G. *Simplified Model for Sodium Coolant Expulsion and Re-entry*, Trans. ANS, *12*(1), 364 (1969).

9. Singer, R. M., "Transient Two-phase Flow Following Sudden Vaporization," *Symposium on Two-phase Flow Dynamics*, Vol. 2, Eindhoven, The Netherlands (Sept 1967) 1683.

10. Singer, R. M., and Holtz, R. E., *On the Role of Inert Gas in Incipient Boiling Liquid Metal Experiments*, Intl. J. Heat Trans. *12*(9), 1045-1060. (1969).

11. Petukhov, B. S., Kovalev, S. A., and Zhukov, V. M., "Study of Sodium Boiling," *Proc. Intl. Heat Transfer Conf.*, Chicago, Vol. 5, 80-91 (1966).

12. Holtz, R. E., and Singer, R. M., *Incipient Pool Boiling of Sodium*, AIChE J. *14*, 654-656 (1968).

13. LeGonidec, B., *et al.*, "Etudes experimentales sur l'ebullition du sodium," *Proc. Intl. Conf. Fast Reactor Safety*, Aix-en-Provence, France (1967).

14. Holtz, R. E., *The Effect of the Pressure-Temperature History upon Incipient Boiling Superheats in Liquid Metals*, ANL-7184 (June 1966).

15. Marto, P. J., and Rohsenow, W. M., *The Effect of Surface Conditions on Nucleate Pool Boiling Heat Transfer to Sodium*, M.I.T. Technical Report No. 5219-33 (Jan 1965).

16. Pinchera, G. C., *et al.*, "Experimental Boiling Studies Related to Fast Reactor Safety," *Proceedings of the International Conference on the Safety of Fast Reactors*, Aix-en-Provence, France (Sept 19-22, 1967).

X